Vortex-mediated bouncing drops on an oscillating liquid

Hong-Yu Chu and Hsiang-Ting Fei
Department of Physics, National Chung Cheng University, ChiaYi 62102, Taiwan
(Received 4 September 2013; revised manuscript received 30 December 2013; published 19 June 2014)

We have investigated the behavior of bouncing drops on a liquid surface by using particle image velocimetry analysis. A drop on an oscillating liquid surface is observed to not coalesce with the liquid and to travel along the surface if the oscillation is strong enough. A streaming vortex pair, induced by the alternatively distorted liquid surface, shows up below a bouncing drop. The time-averaged flow fields of the vortices are measured. In our quasi-one-dimensional setup, there are three stable distances for the drops, which can be characterized by the Faraday wavelength. The interactions of the vortex-mediated bouncing drops are deduced from the streamlines in the liquid bulk. We further show that a three-dimensional vortex ring is induced by a bouncing drop in a square cell.

DOI: 10.1103/PhysRevE.89.063011 PACS number(s): 47.55.dr, 47.32.cb, 47.55.N−, 47.55.P−

I. INTRODUCTION

Acoustic streaming phenomena driven by an oscillating object and obtained from an oscillatory flow have been widely observed and discussed [1–10]. Steady streaming flows are found in various systems, for example, a vortex pair induced by oscillatory flow in a pipe of slowly varying cross section [1,2], oscillating bubble-induced vortex pairs in liquid [3,4], vortex flows observed below the Faraday wave surface [5], a streaming flow propelled boat [6], and the interaction of streaming vortices in liquid [7,8]. The time-averaged streaming flow in an oscillatory fluid is contributed by the nonlinear inertial term $\rho u \cdot \nabla u$ in the Navier-Stokes equations. Longuet-Higgins derived the drift velocity distribution induced by an oscillating spherical bubble in a viscous liquid [10]. With a small amplitude the oscillating gas bubble is capable of inducing vortex flows over a long distance. Marmottant and Hilgenfeldt have shown the modeling of the streaming flow from the oscillating bubble attached to the wall via the images method [4]. In their experiment, the circular streaming flow guides the vesicles moving along in the liquid. The vesicles can be deformed and ruptured by the shear forces in the streaming flow.

The drops bouncing on an oscillating liquid bath and on a soap film are observed to have noncoalescence if the reduced acceleration $\Gamma = 4\pi^2 A f^2/g$ is above a certain threshold, where A is the oscillating amplitude of the bath, f is the oscillating frequency, and g is the acceleration of gravity [11,12]. It is found that the bouncing drops float, travel, and roll on the surface and arrange themselves into a two-dimensional (2D) periodic structure under suitable conditions [12–18]. The noncoalescing drop was investigated by Couder *et al.* [12,13], who confirmed that the thin air layer separates the drop from the liquid bath. Recent investigations suggest that the walking drops are propelled by the normal stress during impact [19–22]. Molacek and Bush [19,20] and Wind-Willassen *et al.* [21] proposed a model where the drop motion is governed by gravity during free flight and by gravity and normal force from the inclined surface during impact. Researchers have successfully predicted the motions of the small drops on the oscillating surface. It was believed that for small walking drops the tangential viscous stress can be negligible due to the low viscosity of air. However, for some large (heavy) drops the asymmetric distortions of the drop and the bath surface should be considered during the impact. Two bouncing drops are also capable of performing a circling motion [14,15], which is explained by considering the interaction of the surface wave and corresponding normal forces. The rolling behavior of the bouncing drops has been reported by Dorbolo *et al.* [16] and Chu *et al.* [17], who imply that the normal force contributed to the drop might not be the only effect.

We report the effects of the surface-induced vortex pairs on the single bouncing drop and on the drop-drop interaction. The vortex streaming patterns in the bulk liquid are revealed with the dye visualization and the particle image velocimetry (PIV) technique. The faster traveling speed of the more viscous drop implies that the shear on the drop might be responsible for the traveling drop. Three stable distances characterized by the Faraday wavelength are found for two drops interacting with each other. The time-averaged PIV analysis and the velocity distribution of the vortex flow corresponding to the conditions of a single drop and three different interacting drop distances are presented. We discuss the tangential force on a heavy drop condition that should not be underestimated for the distortion of the gliding drop and the coupling motion of the drops. We further show that a three-dimensional vortex ring can be induced by a bouncing drop in a square cell.

II. EXPERIMENTAL SETUP

The experiment is conducted in a rectangular acrylic container of 75 mm × 3 mm × 30 mm, which is fixed on a vertically oscillating electromagnetic shaker. The container with such a large aspect ratio is designed to suppress the generation of the Faraday wave in the direction of the camera view (3 mm in depth). Silicone oil (Dow Corning 200) with kinematic viscosity $\nu = 20 \sim 125$ mm^2/s, surface tension $\sigma = 0.0209$ N/m at 25 °C, and density $\rho = 960$ kg/m^3 is used to fill the container and a syringe. The depth of oil bath H is 15 mm. Through syringe injection, drops with a 2 mm diameter are placed on the oscillating oil bath (oscillating frequency $f = 35$–60 Hz). The system is illuminated by 473 nm laser sheets and white light light-emitting diodes (LEDs) and is recorded at 600 frames/s by a commercial camera (Ex-F1,

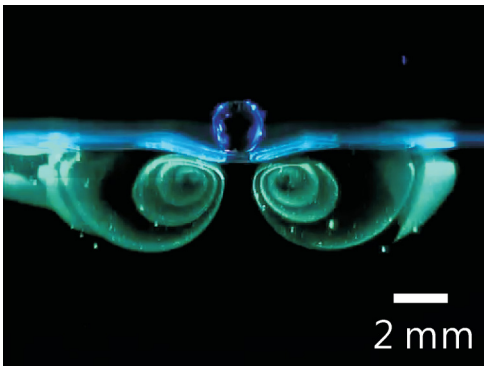

FIG. 1. (Color online) Dye visualization of the vortex pair at one instant in the liquid bath. Two counterrotating vortices are observed after the drop bounces on the liquid surface for a while ($f = 60$ Hz, $\nu = 50$ mm^2/s, and $\Gamma = 6.0$).

Casio). A small amount of the green dye is added to the oil bath to show the vortex flow within the liquid. The volume fraction of the dye is about 1/2000. Some micron-sized carbon particles (diameter of 5 μm, 2.2 g/cm^3) are uniformly distributed in the liquid bulk for PIV measurements (50 particles/mm^3). All images shown in this paper have been acquired with 1 ms exposure. The time-averaged velocity of the fluid is determined in a Lagrangian manner using the displacements of the particles in fluid over one cycle (1/60 s).

III. RESULTS AND DISCUSSIONS

The streaming flow from an oscillating object in a liquid has been observed for years. Here, through the visualization of dye, similar vortex-type streaming flows have also been observed and are shown in Fig. 1. Since it takes time for dye to diffuse and to move, the vortex patterns are formed in the bath after the drop bounces on the surface for a few seconds. While the oil surface is periodically bent and restored, the distorted surface plays the role of the streaming source. The streaming direction underneath the drop is pointing upwards.

The system is contact wetting, and the quasi-one-dimensional oil bath with an aspect ratio of 75:3 provides a thin channel for the drop traveling on the concave liquid meniscus. The gliding drop bounced back and forth within the container, and it did not collide with the sidewalls due to the confinement of the meniscus. Figure 2 shows the shape change of the gliding drop with different viscosities (20–125 mm^2/s). Experiments displayed in Fig. 2 have been conducted at $f = 60$ Hz and below the Faraday wave threshold Γ_F, which is the onset value of the reduced acceleration where the surface becomes unstable. With increasing viscosity, as shown in Figs. 2(a)–2(c), we have observed the elongation of the drop. This is rather surprising since we would expect it would be more difficult for the drop to deform with large viscosity. Figure 2(d) shows that the aspect ratio of the drop increases with viscosity. We have also observed that the drop with larger viscosity travels faster. The shear stress τ is proportional to the velocity gradient and the coefficient of viscosity μ, $\tau_{ij} = \mu \frac{\partial u_i}{\partial x_j}$, where $\nu = \mu/\rho$. As a result, a more viscous fluid provides a stronger shear force on the drop. This leads to the faster traveling and larger deformation of the viscous drop, in agreement with our observation. Note that the degree of distortion of the drop also depends on how close the driving frequency is to the natural frequency of the drop, which is independent of the viscosity of the drop. In the experiments shown in Fig. 2, both the driving frequency and the diameter of the drop have been kept constant at 60 Hz and 2 mm, respectively. With the mass of the drop being fixed, the natural frequency of the drop is also fixed. Therefore the shape change of the drop cannot be caused by the resonance effect.

Furthermore, we observed the interaction of two drops placed on the quasi-one-dimensional liquid bath. Due to the larger distortion of the more viscous drop, we conducted experiments with $\nu = 20$ mm^2/s silicon oil to easily identify the positions of the drops. Three stable positions with two drops at $\Gamma = 3.1$ and $f = 40$ Hz ($\Gamma_F = 4.4$) have been observed, as shown in Figs. 3(a)–3(c). The stable distance d of the drops, governed by the interaction of the bouncing drops, decreases with increasing frequency, shown in Fig. 3(d). Since the surface waves are induced by the bouncing drops, we characterize the distance d in terms of Faraday wavelength λ_F, where $\lambda_F = 2\pi/k_F$, $\omega_F = 2\pi(f/2)$, and $\omega_F^2 = (gk_F + \sigma k_F^3/\rho)\tanh(k_F H)$. There are three characteristic distances as a function of λ_F for the drops, shown in Fig. 3(e); even the surface wave only propagates one-wavelength distance. Similar characteristic distances of the drops were also reported on a planar oscillating liquid bath [18]. We notice that the drops placed far away from each other at the beginning, for example, $d = 3\lambda_F$, are still attracted to each other and stable at about $1.4\lambda_F$. This implies that there should be some mechanism affecting the bouncing drops other than the surface wave.

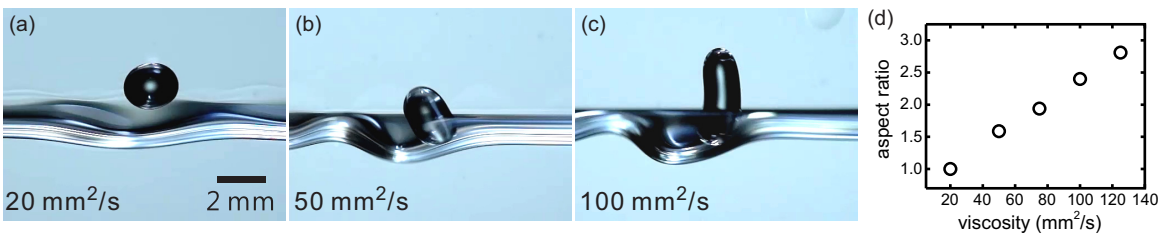

FIG. 2. (Color online) Distortion of the gliding drop with different viscosities. (a)–(c) Larger elongation is observed in more viscous drops. (d) The aspect ratio of the drop increases with viscosity. The elongation and the rotation of the gliding drop imply that there should be a tangential effect acting on the drop.

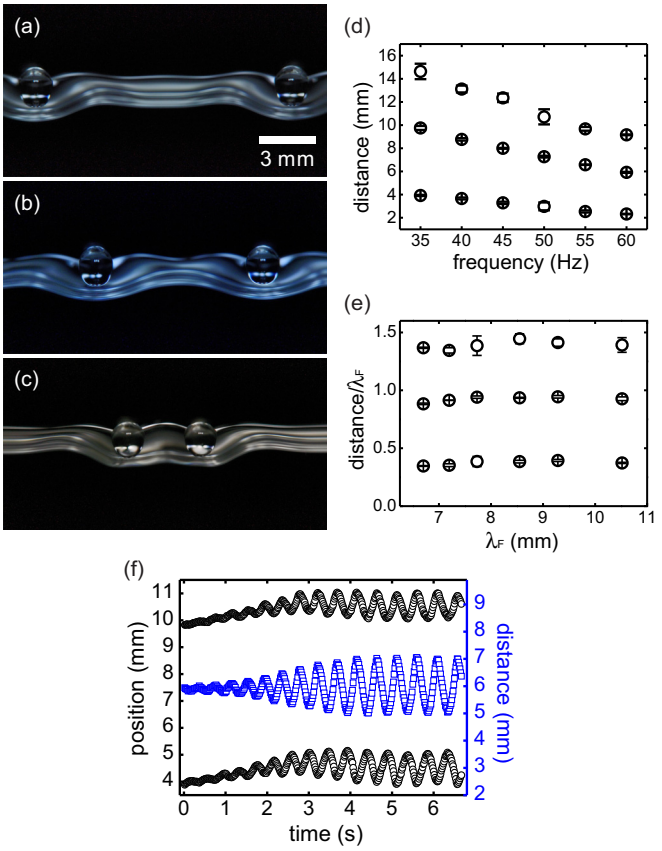

FIG. 3. (Color online) Three stable distances between drops. (a)–(c) show that there are three stable distances for two bouncing drops. Drops are attracting, oscillating, and binding to each other. $f = 40$ Hz and $\Gamma = 3.1$. (d) The three distances decrease with increasing driving frequency. (e) The drop-drop distance normalized by the corresponding Faraday wavelength shows three characteristic values. (f) The positions of the drops (black circles) and the relative distance (blue squares) show that the drops perform an oscillatory motion at about 2.1 Hz with $f = 60$ Hz and $\Gamma = 5.5$ ($\Gamma_F = 6.7$).

We have also observed a coupled oscillation of the drops. Figure 3(f) plots the positions of two drops (black circles) and the distance between the drops (blue squares) as a function of time. After providing a small perturbation on the drop, it is noticed that they perform an oscillating motion without damping at a 2.1 Hz out-of-phase oscillation ($f =$ 60 Hz). The small position deviation can be achieved by a gentle blow on the drops or by a slight increase of Γ (enhanced surface distortion). Oscillations with damping are observed if frequency is below 55 Hz, apparently due to the incoherent oscillation of the surface and the drops. Drops with $0.4\lambda_F$ distance are trapped in the distorted oil surface. The characteristic distance is independent of the oscillating amplitude.

Figure 4(a) shows a PIV measurement of the time-averaged velocity field in the liquid. The time-averaged velocity field and the streaming pattern in the liquid reveal that there is a counter-rotating vortex pair induced on both sides of the bouncing drop. The vortex flows are induced by the alternatively distorted surface as the vortex pairs being generated in the acoustic streaming experiments. Figure 4(b) shows the time-averaged speed in one cycle (1/60 s) along the dashed line marked in Fig. 4(a). The curve fitting is shown as the red line according to the drift velocity distribution of the Lagrangian streaming derived by Longuet-Higgins [10]. The result of the curve fitting suggests the thickness of the Stokes layer $\delta = 0.51$ mm, where in our system $\delta = (2\nu/\omega)^{1/2} = 0.325$ mm. The deviation might come from the large amplitude oscillation of the surface. The velocity profile decreases at longer distance due to the viscous damping.

The time-averaged velocity field and corresponding streamlines of the three equilibrium states of the drops are shown in Figs. 4(c)–4(e) and 4(f)–4(h), respectively. For the drops stabilized at $1.4\lambda_F$, the vortex flows in the inner region are found to repel each other due to the counterrotation of the flows. However, for the drop stabilized at $0.9\lambda_F$, the vortices in the inner region also repel each other, but some of the streaming lines underneath the drops are connected. The streaming lines in the drops with $0.4\lambda_F$ clearly show that the drops bind together, which leads to a wide distorted oil interface. Hence only two counterrotating vortices are observed in this condition instead of four vortices. The vortices appearing in the outer region provide the confining forces to the binding drops. The distorted surface in the center also prevents the collision of the drops (provides the minimum distance), as shown in Fig. 3(c). Our results indicate that, as the impact of the bouncing drop on the liquid bath repeatedly distorts the oil surface, the perturbed surface induces the flows of vortex pairs.

Figures 5(a) and 5(b) show the correlations between the vortices and the traveling drops. The traveling directions of the drops are indicated by the arrows. It is clearly shown that the time-averaged vortex streamlines are asymmetric on two sides of the drop and the dense streamline region falls behind the traveling drop. The presence of asymmetric vortex flows suggests that there are asymmetric shears which guide the motion of the drops. Even though the faster flow (the dense streamline region) is present on one side of the drop, the drop is mostly affected by the shear in the less dense region since most of the contact area lies on this less dense region. The time-averaged speed from the PIV measurement is much smaller than the actual speed at the moment when the drop is landing on the surface (about 100 mm/s near the surface). Given $\tau_{ij} = \mu \frac{\partial u_i}{\partial x_j}$ with $\mu_{\text{oil}} = \rho_{\text{oil}} \nu_{\text{oil}} = 4.8 \times 10^{-2}$ kg m^{-1} s^{-1}, $\mu_{\text{air}} = 1.84 \times 10^{-5}$ kg m^{-1} s^{-1}, the average speed change in oil $\frac{\partial u}{\partial x} \sim (5\,\text{mm/s})/(1\,\text{mm}) = 5\,\text{s}^{-1}$, and the instantaneous speed change in the air layer $\frac{\partial u}{\partial x} \sim (100\,\text{mm/s})/(1\,\mu\text{m}) = 10^5$ s^{-1}, the average shear in oil τ_{oil} is about 0.24 kg m^{-1} s^{-2}, and the shear in thin air upon the sudden landing of the drop τ_{air} is about 1.84 kg m^{-1} s^{-2}. Therefore τ_{air} is estimated to be several times τ_{oil}. The tangential force applied on the drop is estimated according to $F_{\text{air}} = \tau_{\text{air}} A$, with the contact area $A \sim 1$ mm^2, $F_{\text{air}} = 1.84 \times 10^{-6}$ N. Consequently, F_{air} and the effective force on the drop due to the bouncing on an inclined surface are of the same order of magnitude [22].

See the Supplemental Material for the movies of the travel of the gliding drop in the beginning and in the steady state [23]. The sequential snapshots of the drop motion (60 Hz, 50 mm^2/s) in the Supplemental Material [23] show that the drop moved from the left to the right. The frame number is

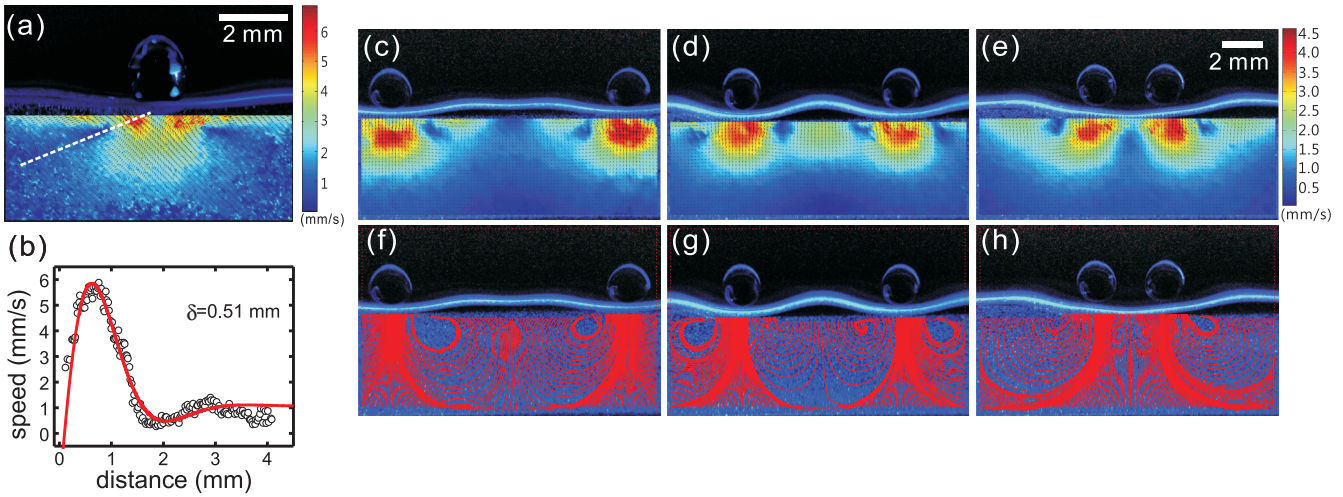

FIG. 4. (Color online) PIV measurement in the liquid bath. (a) Time-averaged velocity field measurement at one instant of a single bouncing drop on the liquid surface. The magnitude of the time-averaged velocity is labeled on the right ($f = 60$ Hz and $\Gamma = 4.9$). (b) Time-averaged flow speed distribution along the dashed line shown in (a). The vortex speed distribution is similar to the result derived by Longuet-Higgins [10]. δ is found to be about 0.5 mm. The time-averaged velocity field and corresponding streamlines of the three equilibrium states of the drops are shown in (c)–(e) and (f)–(h), respectively ($f = 40$ Hz and $\Gamma = 3.1$).

labeled on the corner of the image. From frame 10 to frame 12, we found that most of the contact area lies on the right surface. The normal force from such an inclined surface should stop the drop (pointing in the opposite direction of the motion of the drop). On the contrary, the viscous drop with a large aspect ratio moved faster. The elongated drop is the consequence of the asymmetric vortex flows and the strong shear in the more viscous condition, in agreement with the observation made on the gliding drops in Fig. 2. The shear force might also be responsible for providing the torque of the rotating drop [17].

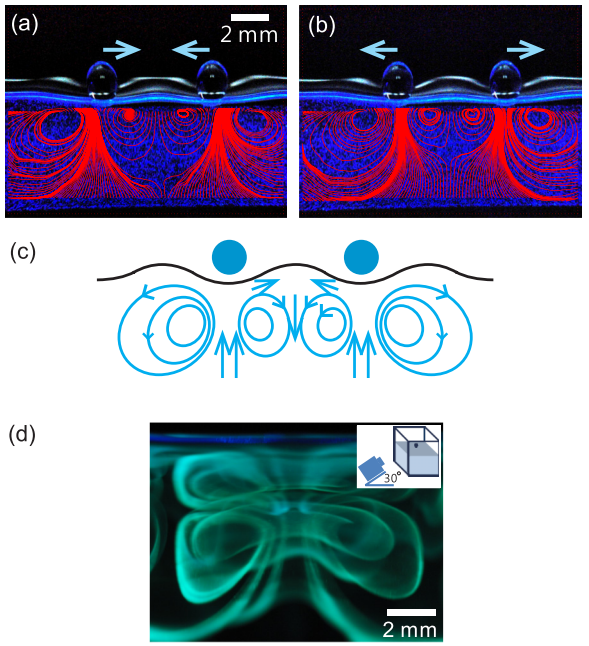

FIG. 5. (Color online) (a) and (b) The time-averaged streamline distributions of the oscillating drops at one instant in time. The traveling directions of the drops are marked by the arrows ($f = 60$ Hz and $\Gamma = 5.5$). It is observed that most of the drop's contact area falls on the less dense streamline region. (c) Illustration of the oscillatory drops and the corresponding flow lines in the liquid. The shears from the vortices are suspected to be responsible for the traveling, rotation, and elongation of the drops. (d) Dye visualization of the vortex ring induced by a bouncing drop on a square liquid bath ($f = 40$ Hz and $\Gamma = 2.4$). The inset shows an illustration of the system setup.

Figure 5(c) illustrates the drops in the oscillating mode. The flow directions are marked by the arrows. The drop becomes stable when the vortices on both sides are in equilibrium. However, once the asymmetry of the vortex flows of a drop becomes large, the drop moves and distorts. This leads to a more distorted surface, which further increases the speed and the distortion of the drop. We have also verified that the vortex ring induced by a bouncing drop (diameter of 1.5 mm) exists in a square cell with a size of 22 mm $\times$ 22 mm $\times$ 30 mm, which is illustrated in the inset in Fig. 5(d). Figure 5(d) shows the dye visualization of the vortex ring (lower one) in the liquid bath at an angle of 30° with respect to the liquid surface. The upper vortex ring is the mirror image reflected by the liquid surface. This observation of the vortex ring in the liquid provides a different view to explain the orbiting drops and the hexagonal pattern of drops discussed in previous investigations [14,15,18].

IV. CONCLUSIONS

We have investigated the interaction between a bouncing drop and an oscillating surface. The vortex-mediated bouncing drops are visualized via dye and the PIV technique. We have shown that the alternatively distorted surface induces a streaming vortex pair in the liquid bulk, which is consistent with the velocity distribution derived by Longuet-Higgins [10]. The mutual interactions of the vortex pairs are associated with the stable positions of the drops. In the process of repeated collisions with the surface, the traveling drop is guided by the shear

force. The elongation and the rotation of the drop should be a consequence of the asymmetric vortex flows and of the strong shear, which become more pronounced in the viscous condition. We have further shown that there is a three-dimensional vortex ring induced by a bouncing drop in a square cell.

ACKNOWLEDGMENTS

We thank F.-K. Men for his suggestions to improve the manuscript. This work is supported by the National Science Council of Taiwan under Contract No. NSC 102-2112-M-194-008-MY3.

[1] P. Hall, J. Fluid Mech. **64**, 209 (1974).
[2] T. M. Squires and S. R. Quake, Rev. Mod. Phys. **77**, 977 (2005).
[3] C. Wang, B. Rallabandi, and S. Hilgenfeldt, Phys. Fluids. **25**, 022002 (2013).
[4] P. Marmottant and S. Hilgenfeldt, Nature (London) **423**, 153 (2003).
[5] E. Martín, C. Martel, and J. M. Vega, J. Fluid Mech. **467**, 57 (2002).
[6] S. K. Chung, K. Ryu, and S. K. Cho, Appl. Phys. Lett. **95**, 014107 (2009).
[7] D. Klotsa, M. R. Swift, R. M. Bowley, and P. J. King, Phys. Rev. E **76**, 056314 (2007).
[8] P. Tho, R. Manasseh, and A. Ooi, J. Fluid Mech. **576**, 191 (2007).
[9] X. Zhao, P. A. Quinto-Su, and C.-D. Ohl, Phys. Rev. Lett. **102**, 024501 (2009).
[10] M. S. Longuet-Higgins, Proc. R. Soc. London, Ser. A **454**, 725 (1998).
[11] T. Gilet and J. W. M. Bush, Phys. Rev. Lett. **102**, 014501 (2009).
[12] Y. Couder, E. Fort, C.-H. Gautier, and A. Boudaoud, Phys. Rev. Lett. **94**, 177801 (2005).
[13] Y. Couder, S. Protiere, E. Fort, and A. Boudaoud, Nature (London) **437**, 208 (2005).
[14] N. Vandewalle, D. Terwagne, K. Mulleners, T. Gilet, and S. Dorbolo, Phys. Fluids. **18**, 091106 (2006).
[15] S. Protiere, S. Bohn, and Y. Couder, Phys. Rev. E **78**, 036204 (2008).
[16] S. Dorbolo, D. Terwagne, N. Vandewalle, and T. Gilet, New J. Phys. **10**, 113021 (2008).
[17] H.-Y. Chu, H.-T. Fei, and C.-R. Ko, Phys. Fluids. **25**, 042101 (2013).
[18] A. Eddi, A. Decelle, E. Fort, and Y. Couder, Europhys. Lett. **87**, 56002 (2009).
[19] J. Molacek and J. W. M. Bush, J. Fluid Mech. **727**, 582 (2013).
[20] J. Molacek and J. W. M. Bush, J. Fluid Mech. **727**, 612 (2013).
[21] Ø. Wind-Willassen, J. Molacek, D. M. Harris, and J. W. M. Bush, Phys. Fluids. **25**, 082002 (2013).
[22] S. Protiere, A. Boudaoud, and Y. Couder, J. Fluid Mech. **554**, 85 (2006).
[23] See Supplemental Material at http://link.aps.org/supplemental/10.1103/PhysRevE.89.063011 for the movies of the travel of the gliding drop in the beginning and in the steady state and the sequential snapshots of the gliding drop in the steady state.